https://doi.org/10.1038/s41567-025-02787-y

Cooperative hydrodynamics accompany multicellular-like colonial organization in the unicellular ciliate *Stentor*

Shashank Shekhar [1,2,3,10] ✉, **Hanliang Guo** [4,5,10], **Sean P. Colin** [2,6], **Wallace Marshall**[3,7], **Eva Kanso** [5,8] ✉ & **John H. Costello** [2,9] ✉

Many single-celled organisms exhibit both solitary and colonial existence. An important step towards multicellularity, which is associated with benefits such as enhanced nutrient uptake, was the formation of colonies of unicellular organisms. However, the initial drivers that favoured individual cells aggregating into more complex colonies are less clear. Here we show that hydrodynamic coupling between proximate neighbours results in faster feeding flows for neighbouring ciliates, such that individuals within a dynamic colony have stronger average feeding flows than solitary individuals. Flows generated by individuals acting together reach higher velocities, thus allowing access to a wider range of prey resources than individuals acting on their own. Moreover, we find that accrued feeding benefits are typically asymmetric: whereas all individuals benefit from acting together, those with slower solitary currents gain more from partnering than those with faster currents. We find that colonial organization in simple unicellular organisms is beneficial for all its members. This provides fundamental insights into the selective forces favouring the early evolution of multicellular organization.

Suspension-feeding unicellular protists inhabit a fluid world dominated by viscous forces that limit prey transport for feeding[1–3]. Many of these organisms generate ciliary microcurrents that actively transport the dissolved nutrients and smaller prey critical for their nutrition[2,4,5]. A protist's ability to favourably alter its feeding current for enhanced feeding would, therefore, be beneficial to its survival. Can colony formation enable unicellular protists to enhance their feeding flows? Colony-forming protists can broadly be classified based on the presence (or absence) of physical linkages between colony members. Organisms, including *Volvox carteri*[2] and the choanoflagellate

Salpingoeca rosetta[6], form colonies of physically attached members that serve as models for studying the evolution of multicellularity[2,7–9]. *Volvox* forms spherical colonies with individual cells embedded within an extracellular matrix jointly secreted by identical, clonal colony members. The combined flows can act over longer distances[10] and transport greater amounts of fluid per individual[10,11], which enables *Volvox* colony members to grow and reproduce faster[12,13].

However, if we step backwards, before these more advanced examples, many colony-forming protists aggregate in high numbers with no observable linkages between colony members. This basal condition

[1]Departments of Physics, Cell Biology and Biochemistry, Emory University, Atlanta, GA, USA. [2]Whitman Center, Marine Biological Laboratory, Woods Hole, MA, USA. [3]Physiology Course, Marine Biological Laboratory, Woods Hole, MA, USA. [4]Department of Mathematics and Computer Science, Ohio Wesleyan University, Delaware, OH, USA. [5]Department of Aerospace and Mechanical Engineering, University of Southern California, Los Angeles, CA, USA. [6]Department of Marine Biology and Environmental Science, Roger Williams University, Bristol, RI, USA. [7]Department of Biochemistry and Biophysics, University of California San Francisco, San Francisco, CA, USA. [8]Department of Physics and Astronomy, University of Southern California, Los Angeles, CA, USA. [9]Department of Biology, Providence College, Providence, RI, USA. [10]These authors contributed equally: Shashank Shekhar, Hanliang Guo. ✉e-mail: shekhar@emory.edu; kanso@usc.edu; costello@providence.edu

mimicking multicellular-like behaviour precedes the evolution of an organizing extracellular matrix or cell–cell junctions, as seen in *Volvox* or choanoflagellates[9]. We, therefore, wondered whether individuals in such a loosely organized colony are capable of coordinating their activity to achieve common goals and whether such cooperation is an exclusive ability of colonies containing physically connected individuals.

To answer this question, we considered two issues: the positioning of individuals in a colony with no common extracellular matrix and the hydrodynamic consequences of such colony formation. Specifically, we chose the ciliated unicellular protist *Stentor coeruleus*. *Stentor* individuals generate feeding currents by beating bands of cilia near their 'heads' at their anterior end and attach onto organic surfaces (such as leaves and twigs in freshwater ponds) with an organelle called a 'holdfast' at their posterior end[14] (Fig. 1a,b). *S. coeruleus* occur as freely swimming individuals under low prey conditions[14]. However, in higher food conditions, *Stentor* individuals can reversibly aggregate into hemispherical colonies by anchoring themselves onto surfaces in close proximity to each other (Fig. 1c). Colony members sway their feeding apparatus back and forth without detaching their holdfast (Supplementary Video 1). We examined the hydrodynamic cooperation between these unconnected colony members and found that, although benefits accrue for neighbouring individuals, the benefits are typically asymmetric between individuals and hydrodynamic cooperation is highly promiscuous among colony members.

Individual *S. coeruleus* freely suspended in water were incubated alone or in groups in a polydimethylsiloxane (PDMS) chamber where they attached to the glass coverslip (Extended Data Fig. 1). Feeding currents generated by the *Stentor* oral cilia[15,16] were visualized by adding a dilute amount of milk and quantified using micro-particle image velocimetry (PIV)[17–19] (Fig. 1d, Supplementary Videos 2 and 3, and Extended Data Fig. 2)[19]. Feeding currents exhibited two symmetric regions of recirculating flows with opposing spin, which we termed 'vortices'. These vortices are probably due to the confinement between two bounding walls in the experimental chamber[20], whereas *Stentors* in the wild are typically bounded only by the substrate to which they attach. The measured flow velocities were the highest (~100 μm s⁻¹) near the oral apparatus, and the magnitude tapered off by an order of magnitude over a distance equivalent to organismal size (~1 mm) (Supplementary Video 4). As only the orthogonal portion of the flow between the two vortices reached the oral opening and could be productively filtered for prey, we defined the feeding flow velocity (U) as the downward velocity component averaged across a line with the same size as the oral opening (Extended Data Fig. 3). The average feeding current velocity of solitary individuals was found to be about 70 ± 18 μm s⁻¹ (±1 standard deviation for $n = 16$) (Extended Data Fig. 4). This velocity corresponds to approximately 3.4×10^3 body volumes cleared per hour, which lies within the 10^3 to 10^6 body volumes per hour range of clearance rates commonly described for protists living in a variety of aquatic environments[19,21]. We observed a threefold difference between the strongest and weakest solitary flows.

When several individuals were incubated, the organisms self-assembled into colonies such that the holdfasts of individuals were anchored on the glass coverslip in close proximity to each other (Fig. 1c,e). This behaviour was conserved in both of the *Stentor* species we examined: *S. muelleri*, which were acquired from their native environment (Fig. 1c), and the laboratory-cultured *S. coeruleus* (Fig. 1e). Unlike solitary individuals, colonies exhibited flow fields with large numbers of complex interfering vortices (Fig. 1e), possibly due to crosstalk between solitary flows of proximate individuals.

To investigate the *Stentor*-generated flows, we built a mathematical model in which the ciliary activity of each *Stentor* was approximated by a point force located at the mouth and pointing inward (Fig. 1f, inset). In our model, a single parameter, the magnitude of the force F exerted on the fluid, subsumes the details of the cilia length, beating frequency and waveform. Dimensional analysis shows that $F \approx \eta U H$, where η is the fluid viscosity, H is the length of a typical *Stentor* (~1 mm)

and U is a typical flow speed (~100 μm s⁻¹). When placed between two no-slip boundaries (as in our experiments), the point force creates two-dimensional recirculating flows in a plane parallel to the bounding walls (Fig. 1f), consistent with theory[22] and empirical observations[20]. Importantly, the confined point-force model faithfully reproduced the experimental flow fields created by solitary (Fig. 1d,f) and colonial individuals (Fig. 1e,g).

To test whether proximity between individuals enhances the feeding flow, we evaluated pairs of *S. coeruleus*. Two individuals attached to a glass coverslip exhibited head movements with respect to each other without altering their anchor locations, so that the head separation distance Δ varied over time. The flow field changed as a function of head separation (Fig. 2a and Supplementary Video 5). As the separation was gradually reduced, their otherwise independent flows with feeding velocities of between 120 and 190 μm s⁻¹ began interacting. The independent vortical structures of the two individuals became asymmetric, with inner vortices decreasing in size (Fig. 2a), until at zero separation ($\Delta = 0$), only two external vortices remained, and the flow field resembled that expected from a *S. coeruleus* much larger than either individual alone (feeding velocity about 330 μm s⁻¹; Fig. 2b,c and Supplementary Video 6). This translates into an asymmetric benefit of ×2.8 and ×1.7 enhancement in feeding flow for the two adjoining individuals, respectively. Hence, the flow enhancements for the two individuals were asymmetric. The weaker individual gained more from the pairing than the stronger one. This pattern was observed across different *Stentor* pairs (Fig. 2d). This was not caused by increased ciliary beating by nearby individuals, as we found no evidence that the frequency of the ciliary waves was altered as the separation distance between individuals was changed (Extended Data Fig. 5).

To better mimic *Stentor* behaviour in the wild, we modelled each *S. coeruleus* as a regularized stokeslet placed near only one wall (Fig. 3a)[20,23–26]. The direction of the force was determined by the inclination angle θ from the vertical plane and a sway angle ϕ in the horizontal plane. When bounded by a single wall, we observed no vortices (Extended Data Fig. 6). Considering $\theta = 0$ (forces perpendicular to the boundary), our model predicted that the combined velocity profile depended upon two main factors: the strengths F_1 and F_2 of the individuals and the separation distance Δ. For pairs of equal strength, the flow field is left–right symmetric for all values of Δ (Extended Data Fig. 7), whereas for individuals of unequal strengths, the flow field was asymmetric (Fig. 3b,c).

How do these asymmetries affect feeding flows of interacting *Stentors*? To compare the gains in pairs of individuals of unequal strengths, we used our mathematical model and employed two quantitative metrics: the average feeding flow U to each *Stentor*, $i = 1, 2$, and a new metric, 'the benefit of being together', which we defined as the difference between the feeding flow when in partnership compared to when in solitary feeding, normalized by the latter, $\text{Benefit}^{(i)} = (U^{(i)}_{\text{pair}}/U^{(i)}_{\text{solitary}} - 1)$.

We conducted two sets of simulations with $\theta = 0$ and $\theta = 0.25\pi$. We found in both cases that, compared with solitary feeding, a *Stentor* gets a net gain in feeding flow rate when placed in close proximity to a partner (Fig. 3d). Importantly, even though each *Stentor* gains by partnering, the relative benefit is asymmetric (Fig. 3g), with the weaker partner benefiting more, as observed experimentally.

Because solitary individuals exhibit a wide dispersion in their flow velocities, we explored a wide range of *Stentor* strength ratio (F_1/F_2) at two different inter-*Stentor* separation distances, $\Delta = 0.05$ and $\Delta = 0.25$ times body length H (1 mm). For all strength ratios, the pair with the smaller separation distance had a higher average feeding flow (Fig. 3e). Additionally, the weaker partner had a higher benefit. Thus, it is always better to be in close proximity to a stronger neighbour (Fig. 3h).

In our model thus far, we assumed parallel individuals, but in our experiments, we found individuals pointing in different directions, and more interestingly, individuals in a colony continuously altering
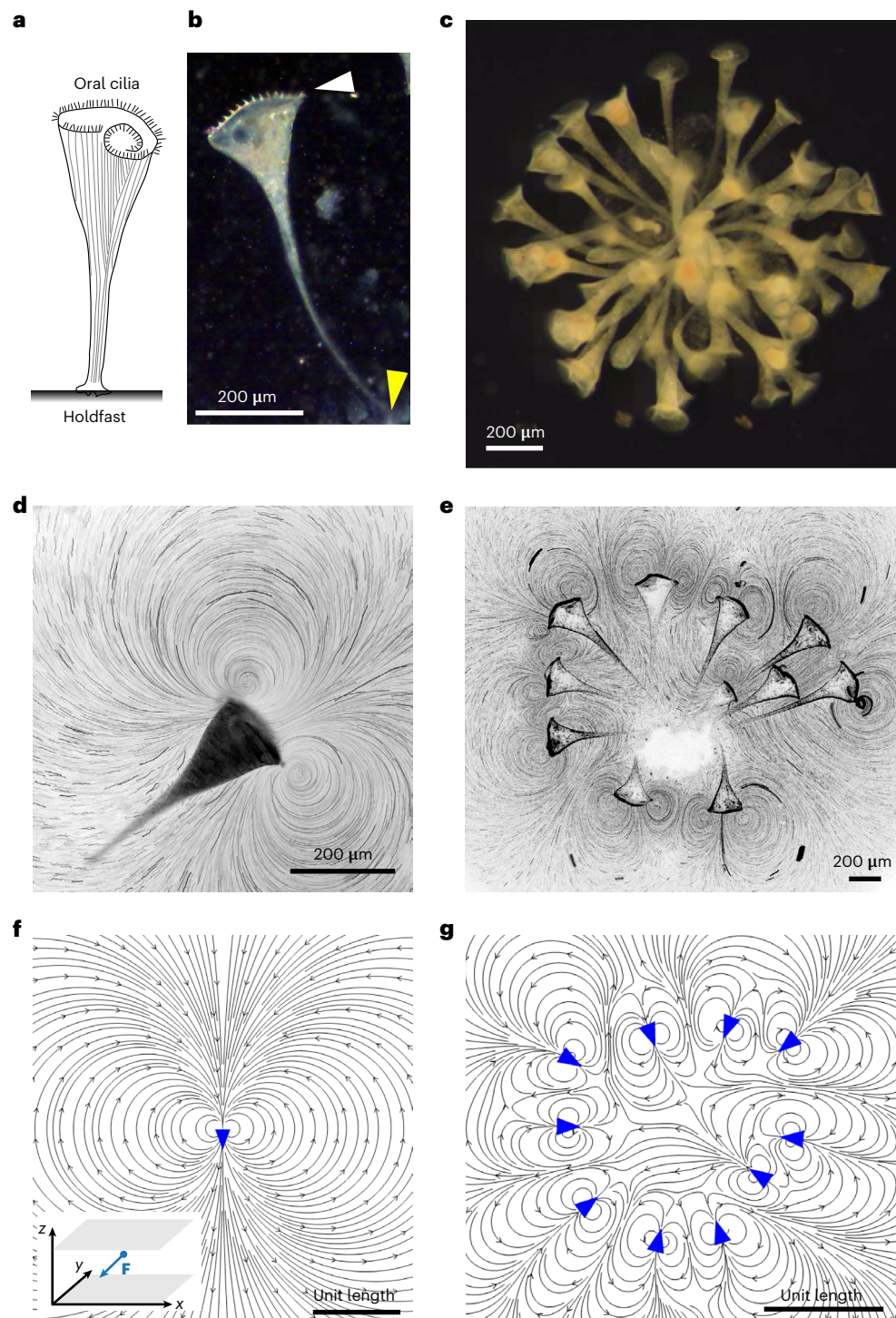
Fig. 1 | Ciliary flows generated by solitary and colonial stentors. a, Schematic representation of *Stentor coeruleus* attached to a surface by a posterior holdfast with an anterior oral ciliary band forming the feeding apparatus (adapted from ref. 15). **b**, Dark-field image of *S. coeruleus* anchored in a PDMS chamber of height 700 μm (Extended Data Fig. 1). The white and yellow arrowheads indicate the ciliary band and the holdfast, respectively. **c**, A self-assembled colony formed by wild *S. muelleri* (Supplementary Video 1). **d,e**, Tracer particle tracks from time-lapse recording of flows generated by an individual *S. coeruleus* (Supplementary Video 3) (**d**) and a colony of 11 *S. coeruleus* (**e**). Outlines of individual colony members can be seen. **f,g**, Streamlines generated by a mathematical model consisting of a single point force (**f**) confined between two bounding walls (inset) and a 'colony' of confined point forces (**g**). The inverted blue triangles denote *Stentor* positions with the wide portion of the triangle representing the individual's oral region. **F** is the strength of the *Stentor*.

not only their positions in the colony but also their orientations (Supplementary Video 1). For a static pair of individuals (same H, Δ and $F_1 = F_2 = F$), the feeding flow rate depends upon the inclination angle θ and sway angle ϕ. Two individuals are cooperative when they point in the same direction and yield positive benefit or antagonistic when they

point in opposite directions and yield negative benefit. However, it is unclear how dynamic changes in orientation and sway angles influence feeding flow rates. To answer this question, we chose $\theta = 0.25\pi$ and added independent Gaussian noises of zero mean to the sway angles ϕ_1 and ϕ_2 to make the individuals deviate from the parallel
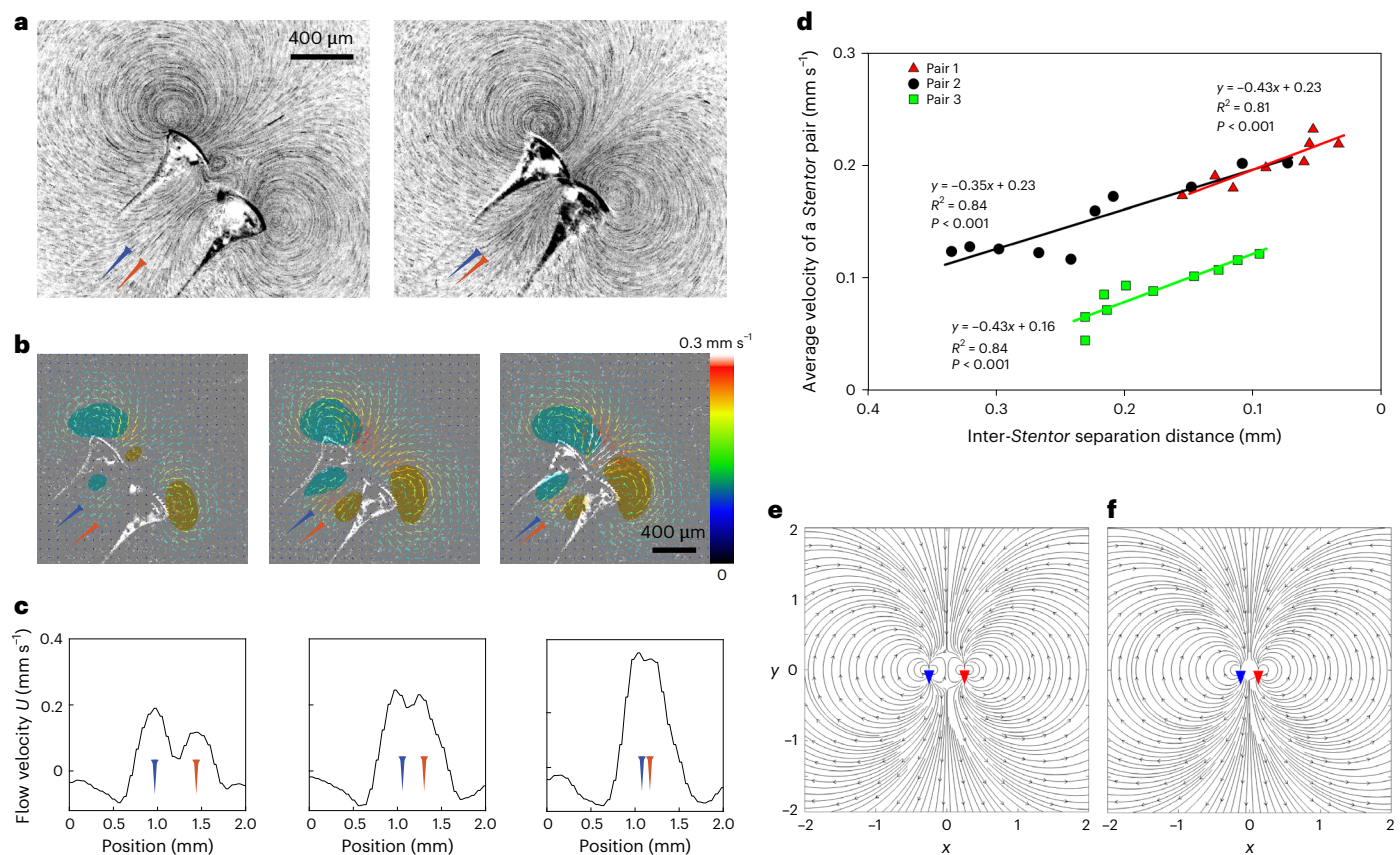
Fig. 2 | Feeding flows in *S. coeruleus* pair increase with decreasing inter-*Stentor* separation. a,b, Flow fields based on particle tracers (**a**) and PIV velocity fields (**b**) for a pair of *S. coeruleus* (with individuals marked as blue or red, respectively) at an intermediate (leftmost) and zero (rightmost) separation distance. Asymmetric outer-inner vortices merge into outer vortices. Indicated are the local flow direction (arrows), flow speed (colour map), and global areas of clockwise (cyan) or anticlockwise (yellow) flow directions (Supplementary Videos 5 and 6). The individuals are visualized by the white outlines in the PIV velocity fields. **c**, Profiles of flow velocity across the two stentors representing instantaneous flow fields at different separation distances corresponding to the images shown in **b**. **d**, Average feeding current velocities for three pairs of *S. coeruleus* increased as the distance between them decreased. Note that the horizontal axis scales from the greatest separation distance on the left to the least distance on the right. As the interindividual distance decreased, the average velocity of both members of the pair increased significantly (all linear regressions, $P < 0.001$). Increased velocities as members of a pair neared each other followed the same pattern. The regression slopes were not significantly different for the three pairs (ANCOVA equal slopes test, 2 degrees of freedom, $P < 0.59$), but the regression intercepts were significantly different (ANOVA for equal slopes, 2 degrees of freedom, $P < 0.001$) due to initial differences between the members of each interacting pair. **e,f**, Flow fields visualized in the plane containing the forces and parallel to the walls for separation distance $\Delta = 0.5$ (**e**) and $\Delta = 0.25$ (**f**). The blue and red triangles represent the positions and orientations of the *Stentor* pair.

configuration. The standard deviation of the sway angle (0.1π) was guided by our experimental observations (Fig. 2b). Using Monte Carlo simulations, we computed the feeding flow rate and benefit to *Stentor* 1 at various strength ratios. Even though the noise had zero mean, the mean feeding flow rate for the Monte Carlo simulations was lower than the feeding flow rate without noise, because the two individuals were most cooperative if $\phi_1 = \phi_2$, and noise drove the pair out of their most cooperative orientation. However, this reduction in mean feeding flow rate and benefit was minimal; the differences between the curves in Fig. 3e,f and Fig. 3h,i are barely noticeable. A standard deviation of 0.1π in the sway angles reduced the feeding flow rate and benefit by only 5%. Adding Gaussian noise to the inclination angles and the separation distance revealed qualitatively similar results (Extended Data Fig. 8).

Given that for a pair of individuals the benefit is asymmetric, if the pairings were permanent, one individual would always be at a loss, thus creating an imbalance. The dynamic nature of *Stentor* colonies (Fig. 4 and Supplementary Video 1) addresses this imbalance by encouraging promiscuity between partners in a colony. We found that within a colony, the nearest neighbour of each member frequently changes (Fig. 4), as there is almost always a neighbour less than 0.25 mm away in a colony (Fig. 4c). Indeed, about 86% of the time, each individual has

a neighbour less than 0.025 mm away and 93% of the time a neighbour less than 0.05 mm away (Fig. 4c). This also explains why organisms in a pair do not always maintain the shortest possible separation to ensure maximal flow rates (Fig. 2). From an evolutionary standpoint, individuals are expected to seek the most favourable energetic pay-off by associating with a neighbouring individual that benefits them the most. One way to accomplish this is to keep switching between neighbouring partners, particularly in a heterogeneous environment when they are changing their location or height in a colony or going through contraction and extension cycles[27,28]. Such an asymmetric advantage favours a dynamic pattern in which colony members continuously change their positions with respect to each other with the result of maximizing their fluid flux. Note that in a colony, an individual moving away from one neighbour will move closer to another neighbour (Fig. 4a). Studying the effect of colony size and organization on feeding flow rates is challenging experimentally. We, thus, extended our model to include N individuals per colony distributed uniformly along a ring of radius equal to H (1 mm) (Fig. 5a, inset), which is like the organization in the inset of Fig. 4c. For non-zero inclination angles, the sway angle of each *Stentor* was chosen such that the force pointed towards the centre of the colony. For small colonies, a reduction in intake velocities occurred
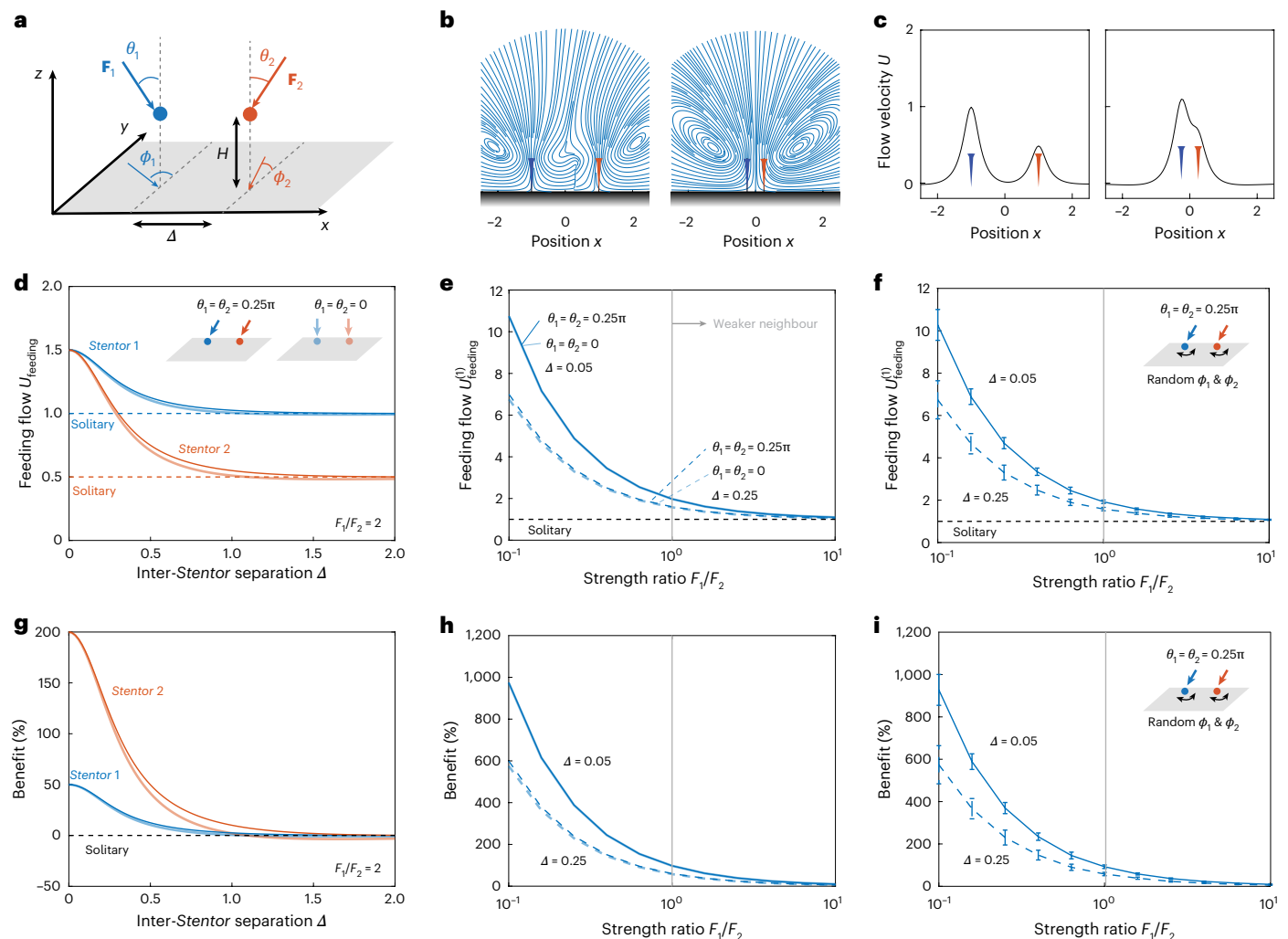
Fig. 3 | Asymmetric feeding benefits in *Stentor* pairs. a, A pair of individuals at a separation distance Δ, modelled as two regularized stokeslets of respective strengths F_1 and F_2 placed at $H = 1$ mm above a no-slip wall. Force directions are determined by their inclinations, θ_1 and θ_2, and sway angles, ϕ_1 and ϕ_2. $\mathbf{F}_1$ and $\mathbf{F}_2$ are the individual strengths of *Stentor* 1 and *Stentor* 2, respectively; H is the length of the *Stentor*. **b**, Flow streamlines constructed in a vertical plane for $F_1 = 1$, $F_2 = 0.5$, $\theta_1 = \theta_2 = 0$, $\Delta = 2$ (left) and $\Delta = 0.5$ (right) with schematic representations of the *Stentors*. **c**, Profiles of the downward flow velocity calculated at $z = 1.25$ with schematic representations of the stentors. **d,g**, Feeding flows (**d**) and benefit of 'being together' (**g**) as functions of Δ. **e,h**, Feeding flow (**e**) and benefit to *Stentor* 1 (**h**) as functions of strength ratio F_1/F_2, given $F_1 = 1$. **f,i**, Mean and standard deviation of feeding flow (**f**) and benefit to *Stentor* 1 (**i**) based on 100 Monte Carlo simulations when the sway angles ϕ_1 and ϕ_2 are subject to Gaussian noise of zero mean and 0.1π standard deviation. **d–h**, $\theta_1 = \theta_2 = 0$ (faint curves). **d–i**, $\theta_1 = \theta_2 = 0.25\pi$ (solid curves). **d–f**, Horizontal dashed lines denote the feeding flow of each *Stentor* in the absence of neighbours. **e,f,h,i**, $\Delta = 0.25$ (dashed curves) and $\Delta = 0.05$ (solid curves). The grey vertical line in the middle separates the cases with a stronger neighbour (left) from those with a weaker neighbour (right).

due to counter flows by stentors on the diametrically opposite side of the colony, but as the colony size was increased, neighbouring forces became more aligned, leading to a higher feeding flow rate (Fig. 5a). When adding Gaussian noise to the *Stentor* positions to mimic dynamic colonies (Fig. 4), we found an enhancement in average feeding rate (Fig. 5b). A similar enhancement was obtained for a range of θ values (Fig. 5b shows only two representative cases to avoid clutter). These results demonstrate that irregular arrangements are advantageous because they create pairs with smaller separation distances.

To date, the benefits of colony formation have been investigated in comparatively advanced organisms, where colony members are either embedded in the same matrix (for example, a *Volvox carteri* colony[2] contains two differentiated cell types held together in an extracellular matrix) or physically attached to each other (for example, *Zoothamnium duplicatum* and choanoflagellate *Codosiga botrytis*[29]). By contrast, *Stentor coeruleus* is a truly unicellular organism, exhibiting a basal-colony-forming behaviour in which unit cells can reversibly

aggregate to form dynamic multicellular-like colonies. Unlike *Volvox*, members of a *Stentor* colony are not physically connected to each other. Our results demonstrate that proximity between individuals is sufficient to enhance the feeding currents. Faster flows can potentially increase the rate of prey encounter and capture and, therefore, provide colony members with a selective advantage over their solitary counterparts. This leads to the question: why would such an organism ever transition back to a solitary state when colonial organization has selective survival advantages? The answer may reflect the pattern among the genus *Stentor* to detach from their colonial organization and swim alone during periods of low prey abundance[14] or to avoid danger[30]. Although detachment from anchoring has been reported to reduce the prey encounter rate by about 30% to 70% for some flagellates (*Pteridomonas danica* and *Paraphysomonas vestita*)[31], it enables rapid swimming and more effective manoeuvring. These traits are valuable for cruising-mode foraging and for avoiding threats. In contrast, *Volvox* colonies cannot disassemble, even under starvation conditions[32].

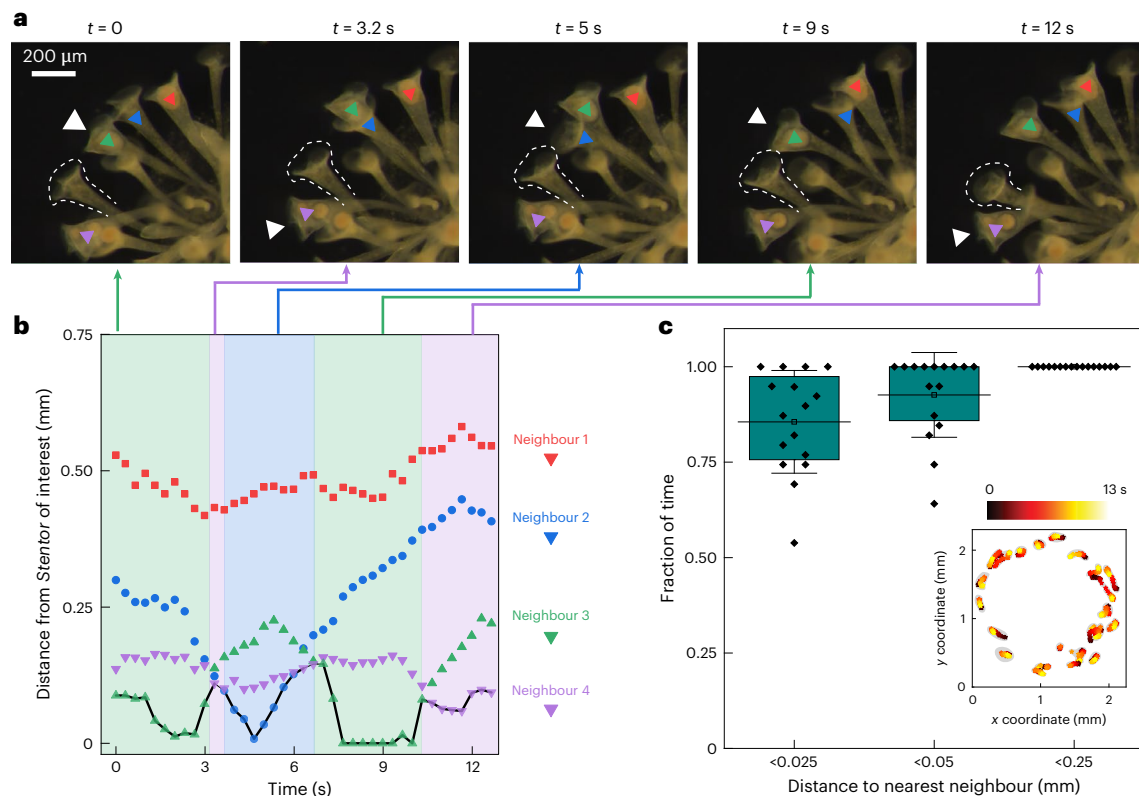**Fig. 4 | Dynamic relocation in a colony encourages nearest neighbour promiscuity. a**, Dark-field images showing five snapshots of a colony of wild *S. muelleri* with five members in the same focal plane, represented by red, blue, green and magenta, with a white arrowhead indicating the closest neighbour to the individual of interest, denoted by the dashed outline. **b**, Time evolution of the distance of each neighbour to the *Stentor* of interest. The closest neighbour changes over time (black line). The vertical coloured boxes along the time axis are colour-coded for the nearest neighbour (denoted by the white arrowhead in **a**) to the individual of interest (denoted by the dashed line in **a**). **c**, Fraction

of total time an individual in a colony has at least one neighbour at a separation distance of less than 0.025, 0.05 or 0.25 mm away. The box plots represent 25/75th percentiles, with the solid line as the mean and whiskers as the standard deviation. Individual points are marked as black diamonds. *n* = 16 pairs. Inset: locations visited by the centre of the oral apparatus. Each grey cluster represents a single individual. Asterisks in a single grey cluster represent the time evolution of a *Stentor*'s location from 0 to 13 s. The colour-coding shows the time progression from *t* = 0 (black) to 13 s (yellow) (Supplementary Video 1 and Fig. 1e).
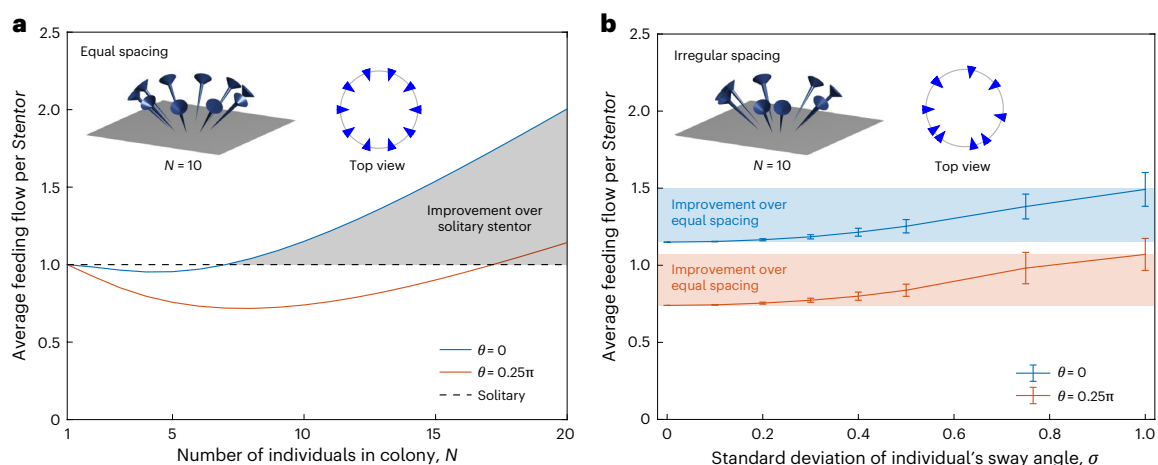

Fig. 5 | Large colony size and dynamic relocation in a colony enhance the feeding flow rate. a, Average feeding flow per individual as a function of colony size in a colony with ten *Stentors* of equal strengths uniformly distributed over a ring of unit radius with individuals pointing towards the centre of the colony (insets). The horizontal dashed line denotes the feeding flow per *Stentor* when the colony has only one *Stentor*. The shaded area highlights the improvement

over the solitary case. **b**, Mean (lines) and standard deviation (error bars) of the average feeding flow per individual from 100 Monte Carlo simulations as a function of standard deviation in their sway angles along the ring. Inclination angle $\theta = 0$ (blue) and $\theta = 0.25\pi$ (red). The shaded areas highlight the improvements over the equal spacing case.

Recent computational studies have reported intriguing relationships between hydrodynamic coupling and feeding flows in choanoflagellate colonies. Although hydrodynamic cooperation between neighbouring choanoflagellates is thought to increase fluid supply to the colony[11], fluid flux across collars of individual choanoflagellates is thought to be greatest when they are freely swimming alone, with sessile colony formation leading to a decreased flux per individual[33]. Unlike choanoflagellates, which are mostly found swimming (alone or in colonies), *Stentors* are normally found attached to surfaces. Importantly, the prediction[11] that in a colony with morphologically similar units the members should arrange themselves in a manner to maximize fluid flux implies that once an optimal arrangement is achieved, it should remain unchanged to ensure the continuation of the maximal benefit. This is true in *Volvox*, where the unit cells remain fixed on a uniform spheroid[10]. Counter-intuitively, we observed that the separation between members oscillates over time, raising the possibility that this oscillatory behaviour might be an inherent property of the organism. Further, differences between *Volvox* and *Stentor* colonies may be influenced by their physical organization. Unlike clonal members of a *Volvox* colony, *Stentors* in a colony do not constitute a homogeneous population and may include a variety of genotypes. Individuals within the same population possess a wide dispersion in size as well as in the velocity of their feeding currents (Extended Data Fig. 4). These disparities between individuals can have major implications for their ability to get the most out of colony formation.

Although we have here assumed that the prey can be treated as small, passive tracer particles, wild *Stentors* feed on smaller motile organisms such as the algae *Chlamydomonas*[14], which themselves swim at speeds of about 100 µm s^{-1} (ref. 34). Successful capture of motile prey would require *Stentors* to generate flow fields with velocities greater than the prey swimming velocity. Our analysis shows that solitary *Stentors* generate flows with an average velocity ~70 µm s^{-1} (Extended Data Fig. 4). As a result, the likelihood that solitary individuals can entrain and capture live prey moving at such high speeds is very low. Notably, our experiments show that stentors in a pair are able to achieve flow velocities two to three times those of *Chlamydomonas* prey velocities.

The dynamic changes in position of individuals within a colony may also alleviate another key challenge for filter feeders attached to surfaces, namely refiltration and recirculation. Recirculation is highest when organisms push liquid perpendicular to the surfaces of their attachment, and even very slow external flows are thought to help overcome challenges associated with flow recirculation[35]. In a *Stentor* colony, however, most individuals are attached at acute angles to the surface and actively vary their position as well as their inclination angle with respect to their attachment surface[26,36] (Fig. 4), indicating that recirculation is not a major issue, even in the absence of external flows, as in our experiments, where individuals remained attached to the glass coverslip for several hours with no external flows.

Taken together, our experimental and modelling analysis shows that although *S. coeruleus* colonial organization appears to be less advanced than that of *Volvox*, the ability of colony members to dynamically alter their morphology and location endows it with very unique benefits. Together, these findings demonstrate that the reversible and dynamic nature of *S. coeruleus* colonies represents a transition between isolated individuals and a coordinated colony that mutually benefits all individuals.

Online content

Any methods, additional references, Nature Portfolio reporting summaries, source data, extended data, supplementary information, acknowledgements, peer review information; details of author contributions and competing interests; and statements of data and code availability are available at https://doi.org/10.1038/s41567-025-02787-y.

References

1. Fenchel, T. Suspension feeding in ciliated Protozoa: structure and function of feeding organelles. *Arch. Protistenkd.* **123**, 239–260 (1980).
2. Goldstein, R. E. Green algae as model organisms for biological fluid dynamics. *Annu. Rev. Fluid Mech.* **47**, 343–375 (2015).
3. Jorgensen, C. B. Comparative physiology of suspension feeding. *Annu. Rev. Physiol.* **37**, 57–79 (1975).
4. Riisgard, H. U. & Larsen, P. S. Particle capture mechanisms in suspension-feeding invertebrates. *Mar. Ecol. Prog. Ser.* **418**, 255–293 (2010).
5. Gilpin, W., Bull, M. S. & Prakash, M. The multiscale physics of cilia and flagella. *Nat. Rev. Phys.* **2**, 74–88 (2020).
6. King, N. The unicellular ancestry of animal development. *Dev. Cell* **7**, 313–325 (2004).
7. Bonner, J. T. The origins of multicellularity. *Integr. Biol.* **1**, 27–36 (1998).
8. van Gestel, J. & Tarnita, C. E. On the origin of biological construction, with a focus on multicellularity. *Proc. Natl Acad. Sci. USA* **114**, 11018–11026 (2017).
9. Grosberg, R. K. & Strathmann, R. R. The evolution of multicellularity: a minor major transition? *Annu. Rev. Ecol. Evol. Syst.* **38**, 621–654 (2007).
10. Short, M. B. et al. Flows driven by flagella of multicellular organisms enhance long-range molecular transport. *Proc. Natl Acad. Sci. USA* **103**, 8315–8319 (2006).
11. Roper, M., Dayel, M. J., Pepper, R. E. & Koehl, M. A. Cooperatively generated stresslet flows supply fresh fluid to multicellular choanoflagellate colonies. *Phys. Rev. Lett.* **110**, 228104 (2013).
12. Solari, C. A., Ganguly, S., Kessler, J. O., Michod, R. E. & Goldstein, R. E. Multicellularity and the functional interdependence of motility and molecular transport. *Proc. Natl Acad. Sci. USA* **103**, 1353–1358 (2006).
13. Koufopanou, V. & Bell, G. Soma and germ: an experimental approach using *Volvox*. *Proc. R. Soc. B: Biol. Sci.* **254**, 107–113 (1993).
14. Tartar, V. *The Biology of Stentor* (Pergamon, 1961).
15. Slabodnick, M. M. et al. The kinase regulator Mob1 acts as a patterning protein for *Stentor* morphogenesis. *PLoS Biol.* **12**, e1001861 (2014).
16. Wan, K. Y. et al. Reorganization of complex ciliary flows around regenerating *Stentor coeruleus*. *Philos. Trans. R. Soc. B* **375**, 20190167 (2020).
17. Kowalczyk, W., Zima, B. E. & Delgado, A. A biological seeding particle approach for µ-PIV measurements of a fluid flow provoked by microorganisms. *Exp. Fluids* **43**, 147–150 (2007).
18. Ukita, H. & Idaka, M. Visualization and analysis of a micro-flow generated by an optical rotator. *Opt. Rev.* **7**, 448–450 (2000).
19. Kanso, E. A., Lopes, R. M., Strickler, J. R., Dabiri, J. O. & Costello, J. H. Teamwork in the viscous oceanic microscale. *Proc. Natl Acad. Sci. USA* **118**, e2018193118 (2021).
20. Pepper, R. E., Roper, M., Ryu, S., Matsudaira, P. & Stone, H. A. Nearby boundaries create eddies near microscopic filter feeders. *J. R. Soc. Interface* **7**, 851–862 (2010).
21. Fenchel, T. in *Nitrogen Cycling in Coastal Marine Environments* Ch. 3 (eds Blackburn, T. H. & Sørensen, J.) 59–65 (Wiley, 1988).
22. Liron, N. & Mochon, S. Stokes flow for a stokes-let between 2 parallel flat plates. *J. Eng. Math.* **10**, 287–303 (1976).
23. Blake, J. R. A note on the image system for a stokeslet in a no-slip boundary. *Math. Proc. Camb. Philos. Soc.* **70**, 303–310 (1971).
24. Blake, J. R. & Otto, S. R. Ciliary propulsion, chaotic filtration and a 'blinking' stokeslet. *J. Eng. Math.* **30**, 151–168 (1996).
25. Cortez, R. The method of regularized stokeslets. *SIAM J. Sci. Comput.* **23**, 1204–1225 (2006).

26. Pepper, R. E. et al. A new angle on microscopic suspension feeders near boundaries. *Biophys. J.* **105**, 1796–1804 (2013).

27. Jones, A. R., Jahn, T. L. & Fonseca, J. R. Contraction of protoplasm. III. Cinematographic analysis of the contraction of some heterotrichs. *J. Cell. Physiol.* **75**, 1–7 (1970).

28. Wood, D. C. Electrophysiological studies of the protozoan, *Stentor coeruleus*. *J. Neurobiol.* **1**, 363–377 (1970).

29. Fenchel, T. Filter-feeding in colonial protists. *Protist* **170**, 283–286 (2019).

30. Dexter, J. P., Prabakaran, S. & Gunawardena, J. A complex hierarchy of avoidance behaviors in a single-cell Eukaryote. *Curr. Biol.* **29**, 4323–4329.e2 (2019).

31. Christensen-Dalsgaard, K. K. & Fenchel, T. Increased filtration efficiency of attached compared to free-swimming flagellates. *Aquat. Microb. Ecol.* **33**, 77–86 (2003).

32. Solari, C. A. et al. Flagellar phenotypic plasticity in volvocalean algae correlates with Peclet number. *J. R. Soc. Interface* **8**, 1409–1417 (2011).

33. Kirkegaard, J. B. & Goldstein, R. E. Filter-feeding, near-field flows, and the morphologies of colonial choanoflagellates. *Phys. Rev. E* **94**, 052401 (2016).

34. Goodenough, U. W. Motile detergent-extracted cells of *Tetrahymena* and *Chlamydomonas*. *J. Cell Biol.* **96**, 1610–1621 (1983).

35. Pepper, R. E. et al. The effect of external flow on the feeding currents of sessile microorganisms. *J. R. Soc. Interface* **18**, 20200953 (2021).

36. Rode, M., Meucci, G., Seegert, K., Kiørboe, T. & Andersen, A. Effects of surface proximity and force orientation on the feeding flows of microorganisms on solid surfaces. *Phys. Rev. Fluids* **5**, 123104 (2020).

Methods

S. coeruleus and *S. muelleri* culturing

S. coeruleus cells were obtained commercially (Carolina Biological Supply) and were subsequently cultured as described earlier[37]. Briefly, cells were grown in the dark at 20 °C in modified *Stentor* medium (0.75 mM Na_2CO_3, 0.15 mM $KHCO_3$, 0.15 mM $NaNO_3$, 0.15 mM KH_2PO_4, 0.15 mM $MgSO_4$, 0.5 mM $CaCl_2$ and 1.47 mM NaCl) modified from recipes by Tartar[14] and De Terra[38]. This medium was supplemented with living prey, *Chlamydomonas reinhardtii*, which were washed in modified *Stentor* medium before being added to the *S. coeruleus* cultures for feeding. A few grains of boiled wheat seeds were also added to the *S. coeruleus* cultures to promote further microbial growth. *C. reinhardtii* cells were added to the *S. coeruleus* cultures two or three times per week.

Stentor colonies in the wild were found attached to fixed solid surfaces including organic matter in freshwater aquatic bodies. *S. muelleri* were taken from Shivericks Pond in Falmouth, MA, United States. About 2 l of pond water along with organic matter, like leaves and twigs, were collected from a shaded part of the pond. The sample was brought back to the laboratory, mixed vigorously by shaking the bottles and then allowed to settle for about 10 min. The water containing the freely swimming organisms was then separated from the organic matter and poured into a borosilicate glass flask. *S. muelleri* were identified under a stereomicroscope and isolated using a P1000 pipette into a separate flask. Filtered pond water was added to the culture, and S. *muelleri* were used in the experiments over the next 24 h.

Microscopy, data acquisition and analysis

Stentors suspended in water mixed with whole milk (diluted ×500) were incubated in a chamber formed by attaching two coverslips onto either side of a PDMS ring 5 mm in diameter and 700 μm high (Extended Data Fig. 1). The patterns illustrated in Figs. 1b,c and 4a were general patterns representative of the ~50 colonies observed in the laboratory. The stentors usually anchored themselves onto the lower glass coverslip attached to the PDMS chamber. Once anchored onto the coverslip, the stentors were imaged in dark field using a ×4 objective on an inverted microscope (Nikon Eclipse TE2000-U) using the software Photron FAST-CAM Viewer (PFV4). The depth of field for this objective was 55.5 μm. The head (oral region) of a *Stentor* is approximately 150 μm wide, so the image focal plane for measuring particle motion represented an optical slice through the three-dimensional space encompassed by the flow field generated by the *Stentor* ciliary bands. When viewing several stentors shifting both inclination angle θ and sway angle ϕ, some flow components occurred outside the measured viewing plane. We minimized this by selecting image sequences in which measured particle flows occurred almost exclusively within the viewing plane. For flow visualization, dark-field time-lapsed images of the anchored stentors with milk particles in their surrounding liquid were acquired at 500 frames per second using a high-speed colour camera (Fastcam 1024 SA3, Photron), such that 1 pixel on the camera corresponded to 4.2 μm. Whether the increase in feeding current velocity associated with pairing also translates into higher prey capture rates was difficult to test because of a *Stentor*'s sensitivity to bright visible light, which prevented us from performing quantitative imaging of prey capture.

Median images were calculated for each video using Fiji and were subtracted from individual video frames to eliminate particles stuck on the surface. These processed images were Z-projected using Fiji to generate images of flow streamlines (Fig. 1c,f). To determine the velocity and vorticity fields, these median-subtracted videos were analysed with a cross-correlation algorithm using DaVis v.8.0 (LaVision). Image pairs were analysed with shifting and overlapping interrogation windows with a size decreasing from 32 × 32 pixels to 16 × 16 pixels. Once the velocity field was measured, the velocity of the feeding current was determined by calculating the average velocity across a line the same size as the oral opening at a distance of 0.25 mm from the oral opening (Extended Data Fig. 3).

Supplementary Videos 3 and 5 were created using the Flowtrace ImageJ plugin from Gilpin et al.[39].

Mathematical modelling of feeding flows

Following common practice in modelling sessile microorganisms, we considered the details of the cilia length, beating frequency and waveform of a *Stentor*'s ciliated ring to be subsumed into a single averaged force that the *Stentor* exerts on the fluid. Specifically, each *Stentor* was modelled by a point force $\mathbf{f}$ pointing in the direction $(\sin\phi\sin\theta, -\cos\phi\sin\theta, -\cos\theta)$ located at position $\mathbf{x} = (x, y, H)$. Geometrically, H stands for the length of the *Stentor* and was kept constant in all of our simulations. θ is the inclination angle between the force and the z axis, such that $\theta = 0$ corresponds to a force pointing perpendicular to the x–y plane. ϕ is the swaying angle between the projection of the force onto the x–y plane and the y axis. We set the regularization parameter a to be $0.2H$, which roughly corresponds to the diameter of the ciliated ring.

The fluid flow generated by a *Stentor* in the model is governed by the incompressible Stokes' equations with zero boundary conditions at the solid wall $z = 0$ and at infinity, namely,

$$-\eta\nabla^2\mathbf{u} + \nabla p = \mathbf{f}\delta(\mathbf{x} - \mathbf{x}_o), \quad \nabla\cdot\mathbf{u} = 0, \quad \mathbf{u}|_{z=0} = 0, \quad \mathbf{u}|_\infty = 0,$$

where $\mathbf{u}$ is the fluid velocity, p the pressure field, η the viscosity of the fluid and δ the three-dimensional Dirac delta function.

To solve for the fluid flow field $\mathbf{u}$, we use the regularized stokeslet method proposed by Cortez[25]. The no-slip wall was realized by adding an appropriate image system to the stokeslet. The image system was originally derived by Blake[23] and was recently reformulated by Gimbutas et al.[40]. The regularized version of the image system was studied by Ainley et al.[41], based on Blake's formulation. The image system consists of the regularized counterparts of a stokeslet, a potential dipole, a Stokes doublet and a rotlet. In general, the fluid velocity at the point $\mathbf{x}_e$ induced by a force $\mathbf{f}$ located at $\mathbf{x}_o = (x_o, y_o, z_o)$ and its images at $\mathbf{x}_{o,im} = (x_o, y_o, -z_o)$ is given by

$$\mathbf{u}(\mathbf{x}_e) = [H_1(r^*)\mathbf{f} + H_2(r^*)(\mathbf{f}\cdot\mathbf{x}^*)\mathbf{x}^*] - [H_1(r)\mathbf{f} + H_2(r)(\mathbf{f}\cdot\mathbf{x})\mathbf{x}] - z_o^2[D_1(r)\mathbf{g}$$
$$+ D_2(r)(\mathbf{g}\cdot\mathbf{x})\mathbf{x}] + 2z_o\left[\frac{H_1'(r)}{r} + H_2(r)\right](\mathbf{f}\times\mathbf{e}_3\times\mathbf{x})$$
$$+ 2z_o\left[H_2(r)(\mathbf{g}\cdot\mathbf{e}_3)\mathbf{x} + H_2(r)(\mathbf{x}\cdot\mathbf{e}_3)\mathbf{g} + \frac{H_1'(r)}{r}(\mathbf{g}\cdot\mathbf{x})\mathbf{e}_3\right.$$
$$\left.+ \frac{H_2'(r)}{r}(\mathbf{x}\cdot\mathbf{e}_3)(\mathbf{g}\cdot\mathbf{x})\mathbf{x}\right],$$

where $\mathbf{x}^* = \mathbf{x}_e - \mathbf{x}_o$, $\mathbf{x} = \mathbf{x}_e - \mathbf{x}_{o,im}$, $r^* = \|\mathbf{x}^*\|$, $r = \|\mathbf{x}\|$, $\mathbf{g} = 2(\mathbf{f}\cdot\mathbf{e}_3)\mathbf{e}_3 - \mathbf{f}$ is the dipole strength, and $H_1(r) = 1/8\pi(r^2 + \epsilon^2)^{1/2} + \epsilon^2/8\pi(r^2 + \epsilon^2)^{1/2}$, $H_2(r) = 1/8\pi(r^2 + \epsilon^2)^{3/2}$, $D_1(r) = 1/4\pi(r^2 + \epsilon^2)^{3/2} - 3\epsilon^2/4\pi(r^2 + \epsilon^2)^{5/2}$ and $D_2(r) = -3/4\pi(r^2 + \epsilon^2)^{5/2}$.

Note there is a typographical mistake in the original paper, which has been corrected in the above expression. We refer interested readers to the aforementioned papers for the derivation of these expressions. A typical flow field of the model *Stentor* for the parameters listed in Extended Data Table 1 is shown in Extended Data Fig. 6. Here, the stokeslet force is scaled as $F \approx \eta U H$.

We determined the feeding flow velocity as the average flux going through a circular disc perpendicular to the force and centred at $\mathbf{x} - (\mathbf{f}/|\mathbf{f}|)d$, where $d = 0.25H$ was a small distance away from the mouth. The diameter of the disc was chosen to be equal to the diameter of the *Stentor*'s mouth. The regularization parameter was also chosen to be equal to the diameter of the *Stentor*'s mouth.

To analyse the performance of a pair of stentors, we used a pair of regularized stokeslets at $\mathbf{x}_1 = (0, 0, H)$ and $\mathbf{x}_2 = (\Delta, 0, H)$, respectively. For the static cases (Fig. 3d,e,g,h), the inclination angles for both stentors were 0 and the sway angles did not matter. For the dynamic cases (Fig. 3f,i and Extended Data Fig. 7), the parameters studied were subject

to Gaussian noise of zero mean ($\sigma = 0.1\pi$ for θ and ϕ, and $\sigma = 0.1$ for Δ). To study the asymmetry between the *Stentor* pair, we kept the strength of the left *Stentor* (F_1) to be constant and varied the strength of the right *Stentor* (F_2) so that $0.1 \leq F_1/F_2 \leq 10$.

U_{solitary} was determined when there was a single *Stentor* in the system, and U_{pair} was determined for each *Stentor* when there were two stentors placed side by side in the system. All feeding flow velocities were scaled by the feeding flow velocity of the solitary *Stentor* 1, whose strength was kept constant.

To analyse the performance of a colony of N stentors, we set the swaying angle of the ith *Stentor* to $\phi_i = 2\pi i/N$ and placed it at $\mathbf{x}_i = (H\cos\phi_i, H\sin\phi_i, H)$ such that the stentors were uniformly placed along a ring of radius H and the projections of their forces pointed towards the centre of the colony. In the dynamic case, we added Gaussian noise to the swaying angle, which perturbed the positions of the stentors along the ring while keeping the forces pointing towards the centre. For all colony cases, the stentors had the same strength.

Reporting summary

Further information on research design is available in the Nature Portfolio Reporting Summary linked to this article.

Data availability

Data supporting the findings of this paper are available from the corresponding authors upon reasonable request. Source data are provided with this paper.

Code availability

Code developed as part of this work will be available from the corresponding authors upon reasonable request.

References

37. Slabodnick, M. M. et al. The macronuclear genome of *Stentor coeruleus* reveals tiny introns in a giant cell. *Curr. Biol.* **27**, 569–575 (2017).
38. De Terra, N. Culture of *Stentor coeruleus* on *Colpidium campylum*. *J. Protozool.* **13**, 491–492 (1966).
39. Gilpin, W., Prakash, V. N. & Prakash, M. Flowtrace: simple visualization of coherent structures in biological fluid flows. *J. Exp. Biol.* **220**, 3411–3418 (2017).
40. Gimbutas, Z., Greengard, L. & Veerapaneni, S. Simple and efficient representations for the fundamental solutions of Stokes flow in a half-space. *J. Fluid Mech.* **776**, R1 (2015).
41. Ainley, J., Durkin, S., Embid, R., Boindala, P. & Cortez, R. The method of images for regularized stokeslets. *J. Comput. Phys.* **227**, 4600–4616 (2008).

Author contributions

S.S. and J.H.C. designed the experiments. H.G. and E.K. designed the mathematical model. S.S. conducted the experiments. H.G. performed the simulations. S.S., S.P.C. and W.M. analysed the experimental data. H.G. and E.K. analysed the model results. S.S., J.H.C., H.G. and E.K. put together all the results and wrote the paper.

Competing interests

The authors declare no competing interests.

Additional information

Extended data is available for this paper at https://doi.org/10.1038/s41567-025-02787-y.

Supplementary information The online version contains supplementary material available at https://doi.org/10.1038/s41567-025-02787-y.

Correspondence and requests for materials should be addressed to Shashank Shekhar, Eva Kanso or John H. Costello.

Peer review information *Nature Physics* thanks the anonymous reviewers for their contribution to the peer review of this work.

Reprints and permissions information is available at www.nature.com/reprints.
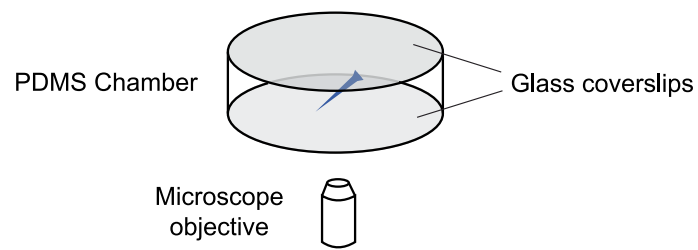
Extended Data Fig. 1 | Experimental setup for visualizing empirical flowfields. Schematic representation of the imaging chamber formed by attaching two coverslips on either side of a polydimethylsiloxane (PDMS) ring 5 mm in diameter and 700 μm high. The microscope is positioned below the PDMS chamber. *Stentors* (blue schematic) usually anchored themselves on the lower glass coverslip attached to the PDMS chamber.
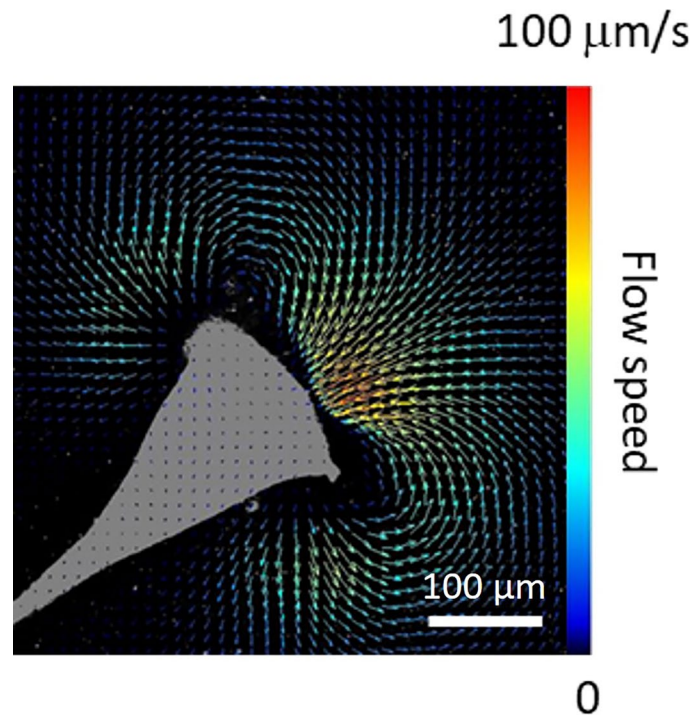
Extended Data Fig. 2 | PIV analysis to measure flow velocity of solitary *Stentor* individuals. Particle image velocimetry (PIV) analysis of the flow generated by the organism (gray shaded area) shown in Fig. 1d (also see supplementary video 4). The direction of the arrows denotes the local flow direction and color denotes the magnitude of the flow speed.
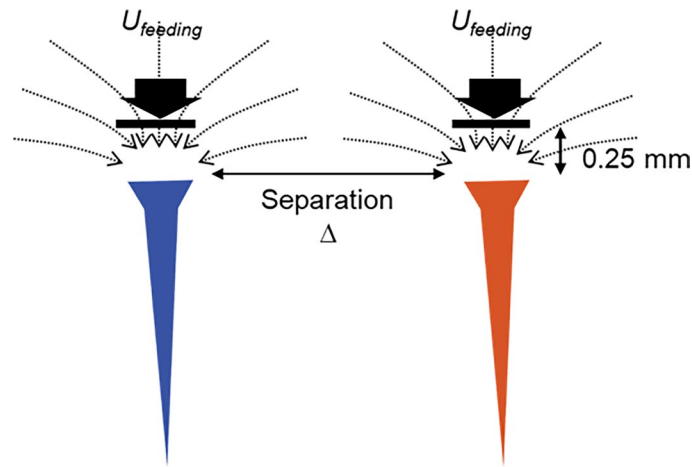
Extended Data Fig. 3 | Methodology for measurement of feeding currents. Since only the orthogonal portion of the flowfields in the region between the two vortices reaches the oral opening and can be productively filtered for prey, only the velocity component normal to the oral opening, $U_{feeding}$ (thick black arrow), is taken as a measure of the feeding current. Due to mixing between tracer and cilia movements, feeding current velocities were measured 0.25 mm from the oral opening to prevent contamination of the PIV analysis due to its inability to separate tracer movements from ciliary beating. Feeding current ($U_{feeding}$) for each individual in a pair or alone was determined by calculating the average velocity across a line the size of the oral opening of each individual. Thin black arrows denote the flow streamlines. Thin double-headed arrow denotes separation between the two *Stentors*. Thick arrow denotes the flow directed towards the oral opening of each *Stentor*.
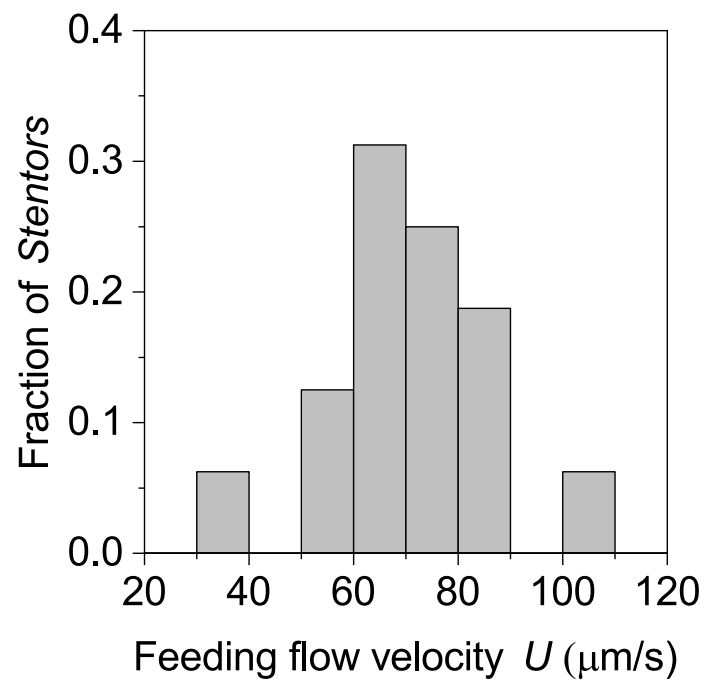
Extended Data Fig. 4 | Feeding current velocities of solitary individuals. Distribution of velocities of the feeding current generated by solitary *Stentor* individuals (n = 17) measured at 0.25 mm from the ciliary band.
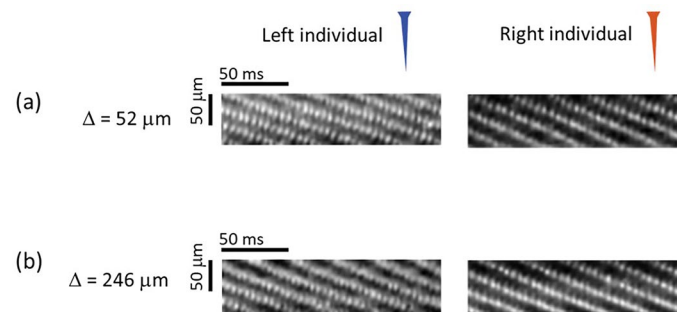
Extended Data Fig. 5 | Ciliary wave velocity remains unchanged with proximity. Kymographs showing the frequency of the metachronal waves for the two individuals in the pair shown in Fig. 2a,b. The frequency of the metachronal wave for the left and the right *S. coeruleus* in the pair remains unchanged as the distance, Δ, between the two individuals changes from (**a**) Δ = 52 μm (left: 16.7 Hz, right: 15.4) to (**b**) Δ = 246 μm (left: 16.6 Hz, right: 15.2 Hz).
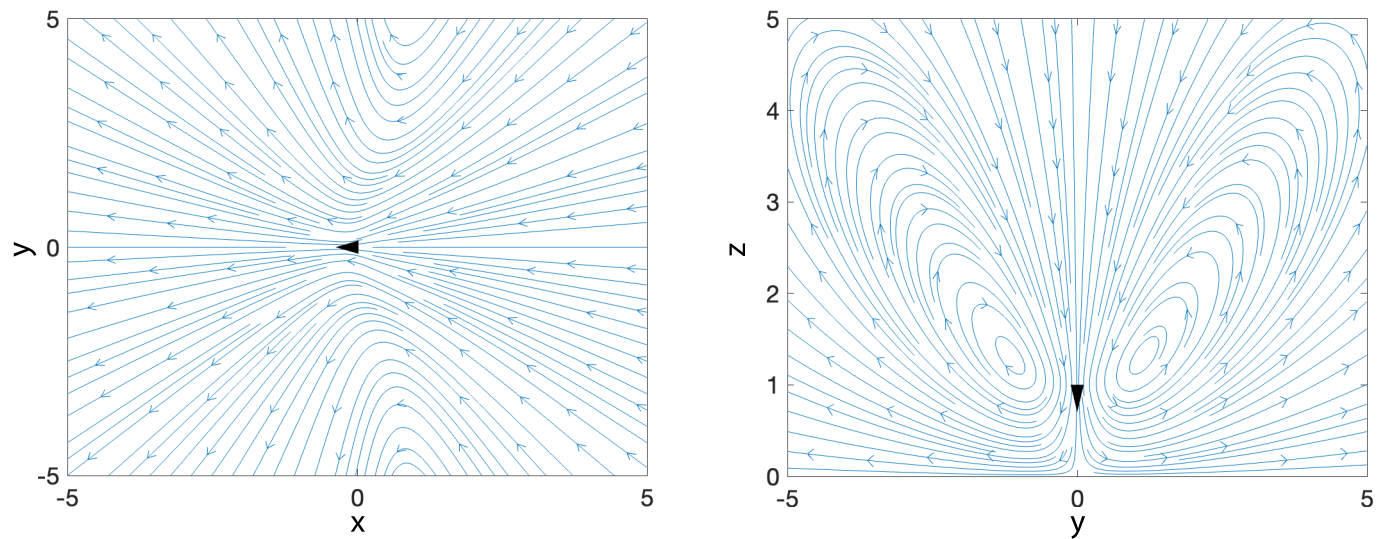
Extended Data Fig. 6 | Streamlines generated by the model *Stentor*. Flow fields of a single *Stentor* modeled as a regularized force (black arrowhead) bounded by one wall (θ = 0.25π), viewing from above (left panel) and from side (right panel). Blue lines and arrows denote the streamlines and the direction of the flow.

(a) *Stentors* with equal strength ($F_1 / F_2 = 1$)

(b) *Stentors* with unequal strength ($F_1 / F_2 = 2$)
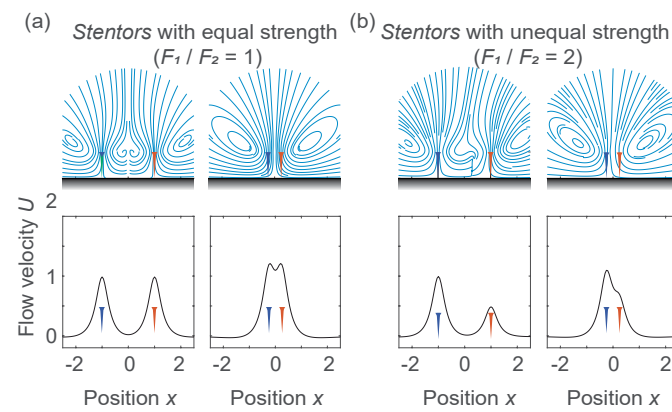
Extended Data Fig. 7 | Streamlines generated by a pair of model *Stentor* individuals. (**a**) Fluid flows generated by a *Stentor* pair, modeled as a pair of regularized Stokeslets of strengths F_1 and F_2 respectively near a wall with force ratio $F_1/F_2 = 1$, inter-*Stentor* separation distance $\Delta = 2$ (left) and $\Delta = 0.5$ (right)

(**b**) Force ratio $F_1/F_2 = 2$ and inter-*Stentor* separation distances $\Delta = 2$ (left), and $\Delta = 0.5$ (right). Top row: flow streamlines. Bottom row: downward velocity component of the flow velocity determined along the horizontal line $z = 1.25H$.
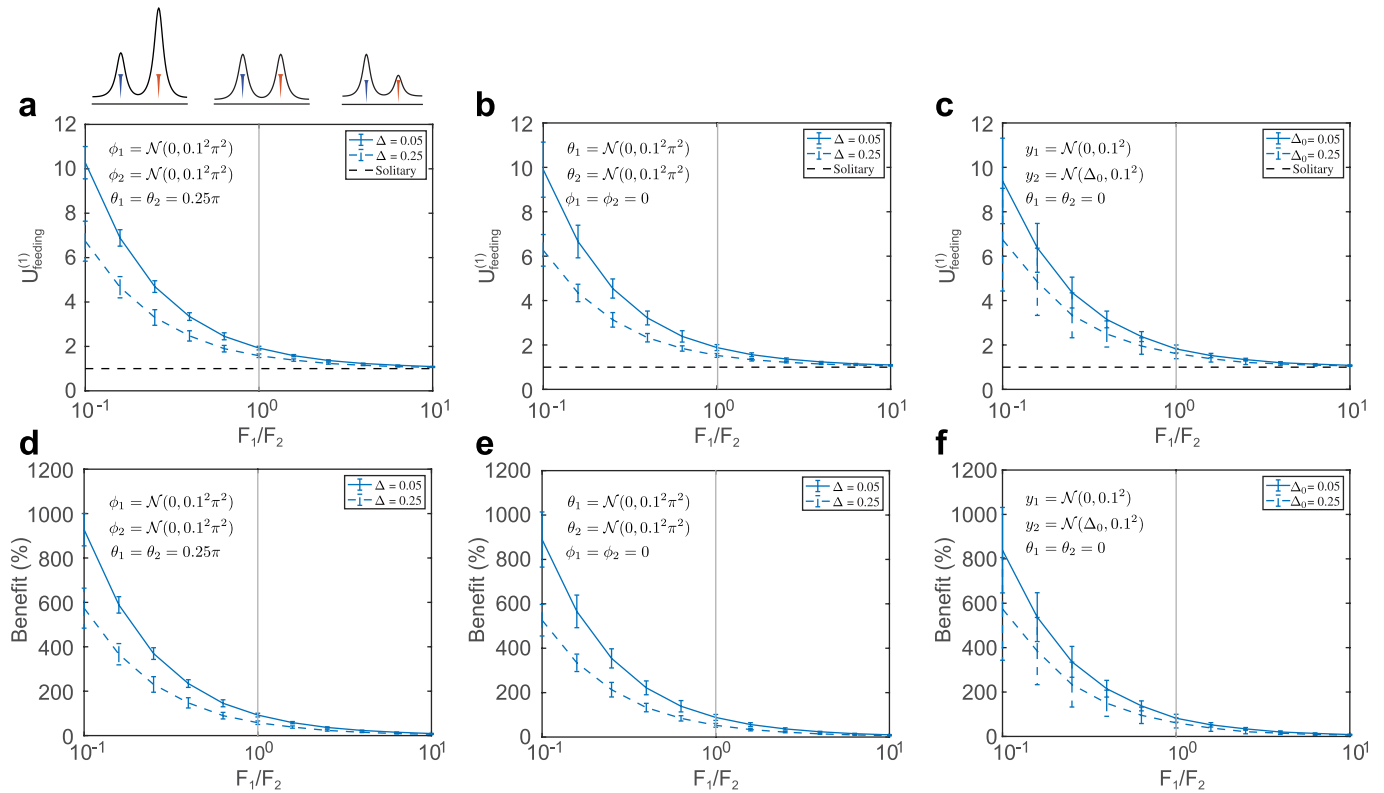
Extended Data Fig. 8 | Feeding flow rate and the benefit for individual *Stentor* in a pair. (a-c) Feeding flow rate of *Stentor* 1 U(1)$_{feeding}$ in a *Stentor* pair whose swaying angles $\phi_{1,2}$ (**a**), inclination angles $\theta_{1,2}$ (**b**), and the separation distances Δ (**c**) are subject to Gaussian noises. The horizontal dashed lines represent the feeding flow rate of solitary *Stentor*. The gray vertical lines separate the cases of having a stronger neighbor (left) and weaker neighbor (right), same as in (**d**–**f**). (**d-f**) The benefit of "being together" for *Stentor* 1 in a *Stentor* pair whose swaying angles (**d**), inclination angles (**e**), and the separation distances (**f**) are subject to Gaussian noises. The mean (lines) and the standard deviations (error bars) are obtained from 100 Monte Carlo simulations. F_1 and F_2 are the individual strengths of *Stentors* 1 and 2.

Extended Data Table 1 | Characteristic scales of the Stokeslet model

Parameter	Symbol	Dimensional value
Stentor height	H	1 mm
Fluid viscosity	η	10^{-3} Pa s
Flow velocity	U	100 µm s^{-1}

Extended Data Table 1 | Characteristic scales of the Stokeslet model

nature portfolio

Corresponding author(s): Shashank Shekhar

Last updated by author(s): Dec 18, 2024

Reporting Summary

Nature Portfolio wishes to improve the reproducibility of the work that we publish. This form provides structure for consistency and transparency in reporting. For further information on Nature Portfolio policies, see our Editorial Policies and the Editorial Policy Checklist.

Statistics

For all statistical analyses, confirm that the following items are present in the figure legend, table legend, main text, or Methods section.

n/a	Confirmed	
☐	☒	The exact sample size (*n*) for each experimental group/condition, given as a discrete number and unit of measurement
☐	☒	A statement on whether measurements were taken from distinct samples or whether the same sample was measured repeatedly
☐	☒	The statistical test(s) used AND whether they are one- or two-sided *Only common tests should be described solely by name; describe more complex techniques in the Methods section.*
☒	☐	A description of all covariates tested
☒	☐	A description of any assumptions or corrections, such as tests of normality and adjustment for multiple comparisons
☐	☒	A full description of the statistical parameters including central tendency (e.g. means) or other basic estimates (e.g. regression coefficient) AND variation (e.g. standard deviation) or associated estimates of uncertainty (e.g. confidence intervals)
☐	☒	For null hypothesis testing, the test statistic (e.g. F, t, r) with confidence intervals, effect sizes, degrees of freedom and P value noted *Give P values as exact values whenever suitable.*
☒	☐	For Bayesian analysis, information on the choice of priors and Markov chain Monte Carlo settings
☒	☐	For hierarchical and complex designs, identification of the appropriate level for tests and full reporting of outcomes
☒	☐	Estimates of effect sizes (e.g. Cohen's *d*, Pearson's *r*), indicating how they were calculated

Our web collection on statistics for biologists contains articles on many of the points above.

Software and code

Policy information about availability of computer code

Data collection	Photron FASTCAM Viewer 4 software was used for image acquisition.
Data analysis	Following software were used for data analysis: 1. Fiji 2. LaVision DaVis

For manuscripts utilizing custom algorithms or software that are central to the research but not yet described in published literature, software must be made available to editors and reviewers. We strongly encourage code deposition in a community repository (e.g. GitHub). See the Nature Portfolio guidelines for submitting code & software for further information.

Data

Policy information about availability of data

All manuscripts must include a data availability statement. This statement should provide the following information, where applicable:
- Accession codes, unique identifiers, or web links for publicly available datasets
- A description of any restrictions on data availability
- For clinical datasets or third party data, please ensure that the statement adheres to our policy

Data supporting the findings of this manuscript are available from the corresponding author upon reasonable request.

Human research participants

Policy information about studies involving human research participants and Sex and Gender in Research.

Reporting on sex and gender	NA
Population characteristics	NA
Recruitment	NA
Ethics oversight	NA

Note that full information on the approval of the study protocol must also be provided in the manuscript.

Field-specific reporting

Please select the one below that is the best fit for your research. If you are not sure, read the appropriate sections before making your selection.

☒ Life sciences ☐ Behavioural & social sciences ☐ Ecological, evolutionary & environmental sciences

For a reference copy of the document with all sections, see nature.com/documents/nr-reporting-summary-flat.pdf

Life sciences study design

All studies must disclose on these points even when the disclosure is negative.

Sample size	Samples for the empirical measurement of flow fields were based on individual Stentors of variable size and flow speeds. Due to the inherent differences between individuals and the variable inter-individual distances in a dynamically moving colony, replication of pre-determined intervals was not an appropriate statistical approach to describe these interactions. Instead, we used regression analysis to measure continuous variation in flows accompanying the dynamic variations between individuals and their relative positions. For this approach, we replicated the patterns and used analysis of covariance between significant regressions to evaluate the empirical patterns (e.g. Fig 2d). Sample collection was sufficient to result in statistically significant results both within and between cases.
Data exclusions	No Stentor data that we collected was excluded from analysis.
Replication	All experiments presented in the manuscript were repeated at least three times. Replication yielded successfully replicable patterns as demonstrated by similar regression slopes for flow speed vs inter-Stentor distances.
Randomization	Individual Stentors possessed variable flow speeds and the distances between individuals varied dynamically during the course of measurement. Hence, the dynamic nature of the system being measured did not necessitate further design randomization.
Blinding	Blinding involves ensuring that researchers collecting and analyzing data are unaware of the treatment or experimental group of the samples to prevent bias. In this study, blinding was implemented wherever possible during data analysis to maintain objectivity. Given the nature of the experimental system, certain aspects of blinding were not applicable

Reporting for specific materials, systems and methods

We require information from authors about some types of materials, experimental systems and methods used in many studies. Here, indicate whether each material, system or method listed is relevant to your study. If you are not sure if a list item applies to your research, read the appropriate section before selecting a response.

Materials & experimental systems

n/a	Involved in the study
☒	Antibodies
☒	Eukaryotic cell lines
☒	Palaeontology and archaeology
☒	Animals and other organisms
☒	Clinical data
☒	Dual use research of concern

Methods

n/a	Involved in the study
☒	ChIP-seq
☒	Flow cytometry
☒	MRI-based neuroimaging